

Electronic and magnetic properties of $\text{NiS}_{2-x}\text{Se}_x$: a comparative study

Cosima Schuster

Institut für Physik, Universität Augsburg, 86135 Augsburg, Germany

Received: date / Revised version: date

Abstract. The metal-insulator transition and the problem of d -electron delocalization are investigated in the pyrite system $\text{NiS}_{2-x}\text{Se}_x$ under pressure using density functional theory (DFT). We test several approximations, including the generalized gradient approximation (GGA), the GGA+ U approach, and hybrid functionals. In addition we apply the GW approximation and perform Hartree-Fock calculations. The important role of the chalcogen dimers in the electronic structure is discussed within GGA, which sufficiently describes the role of the lattice in the metal-insulator transition. In addition, the magnetic phase diagram is determined. However, the electronic properties are inadequately described – the insulating ground state of NiS_2 cannot be obtained – and the magnetic order is slightly overestimated. If correlations are taken into account within GGA+ U , the insulator is found, but the non-magnetic ground state of the doped samples is not accessible. Mixing Fock exchange with local approximations as GGA correctly reproduce the insulating ground state in NiS_2 , and metallic ground states with doping and pressure. The insulator is – in contrast to earlier suggestions – of Mott type, i. e. the gap opens between Ni $3de_g$ states. Due to the Fock term, the magnetic order is strongly overestimated. The applied GW calculations are not able to correct the metallic character of NiS_2 and underestimate the gap by one order of magnitude.

PACS. 71.15.Mb Density functional theory, local density approximation, gradient and other corrections – 71.20.Be Electron density of states and band structure of transition metals – 71.30.+h Metal-insulator transitions and other electronic transitions

1 Introduction

Crystal field splitting, electron-electron interaction, and the $3d$ band width are almost equal in the pyrites MX_2 ($\text{M}=\text{Fe},\text{Co},\text{Ni},\text{Cu},\text{Zn}$; $\text{X}=\text{S},\text{Se}$) which gives rise to a large variety of electrical, magnetic and optical properties in these compounds. Of special interest is the metal-insulator transition in NiS_2 with Se-doping [1] or under pressure [2]. The transition is not accompanied by a change in the lattice symmetry and is commonly believed to be driven by the electron-electron interaction. In addition, a low-temperature antiferromagnetic phase is observed both in the insulating and metallic regime of $\text{NiS}_{2-x}\text{Se}_x$ [1] and by applying pressure in NiS_2 [3]. The electronic and optical properties of NiS_2 were first investigated already 30 years ago [4], and re-investigated experimentally in the late nineties [5,6,7,9,8]. The renewed interest in transition-metal oxides and their metal-insulator transitions traces back to the attempt to understand the phase diagram of the high- T_c superconducting perovskites. Moreover, the attempt to use the metal-insulator transition of V_2O_3 or VO_2 for technical applications triggered many studies up to now [10].

Theoretical attempts using density functional theory and the local density approximation (LDA) to describe the electronic structure of the pyrites date back to 1987 [11], with the focus on FeS_2 , where the important role of the $\text{S}(\text{e})\text{-S}(\text{e})$ dimers present in the pyrite structure has been pointed out. The role of electron-lattice interaction when applying pressure was studied ten years later, again in FeS_2 [12]. Other pyrites are mentioned in [11], and their

electronic structure is explained by filling the band structure with the d -electrons of the transition metal by going from Fe ($3d^6 4s^2$) to Zn ($3d^{10} 4s^2$). The band insulators are described quite well within the local density approximation. However, the microscopic origin of the insulating nature of NiS_2 is not well understood. Since more advanced approximations within DFT are available now, several attempts to improve the material specific theory have been performed. Recently, Perucchi *et al.* [13] have discussed two different mechanisms for the metal-insulator transitions based on LDA calculations. Compression and expansion of the lattice alter the metallic state, albeit through two different microscopic mechanisms. On the other hand, Kuneš *et al.* [14], using LDA+DMFT, have traced back the metal-insulator transition to a single control parameter, namely the size of the p gap. They confirmed, however, that compression and doping influences this control parameter in different ways. Both studies concentrate on the electronic structure in the paramagnetic phase and neglect the magnetism.

Hence, we clarify the role of the S-S dimers and discuss the energy scales mentioned in [13,14]. For the calculations we use the wien2k code [15] and the generalized gradient approximation (GGA) in the parameterization of PBE [16]. In a next step we determine the magnetic phase diagram, Sec. III. Surprisingly, GGA describes the magnetic phase diagram quite well, slightly overestimating the phase boundaries as compared to experimental data. In contrast to GGA, LDA always favors the non-magnetic ground state. Calculations using improved

exchange-correlations functionals are presented in Sec. IV. We present results of GGA+ U (SIC) [17] and EECE hybrid [18,19] calculations. To compare with we have performed also GW calculations on top of LDA using ABINIT [20,21]. We focus on the advantages and shortcomings of the different techniques with regard to correlated materials.

2 The role of the dimers for the electronic structure

The pyrite structure is a simple cubic lattice with space group $\text{Pa}\bar{3}$. It is best described in terms of the NaCl structure with the transition metal in one sub-lattice and the center of mass of the chalcogenide pairs in the other. Thus, the S/Se atoms form distorted octahedra around the Ni atoms. In the following, we use the experimental lattice constant of NiS_2 , $a = 5.687 \text{ \AA}$ [22]. Applying hydrostatic pressure is simulated by a shortening of the lattice constant – 5 %/10 % volume reduction correspond to 1.7 %/3.5 % reduction of the lattice constant and to 5/12 GPa, respectively. In the attempt to understand the phase diagram with doping we concentrate on the end points with $x = 0$ and $x = 2$. In addition we consider also $x = 1$, i. e. NiSSe . For NiSe_2 we also use the experimental lattice constant, $a = 5.960 \text{ \AA}$ [22]. In case of NiSSe , we study two different configurations within the pyrite unit cell – recent STM measurement on doped samples show no sign of a superstructure [23] – and use the theoretically obtained volume, $a_{\text{theo}} = 5.87 \text{ \AA}$ which is about 1 % larger than

estimated in experiments [24,1]. The first configuration contains S_2 and Se_2 dimers, the second only S–Se pairs. Thereby the second configuration is favored by 0.015 Ryd when the volume is fixed. In general, S-S, S-Se, and Se-Se pairs are present in doped samples [8].

Using the mentioned lattice constants the internal positions are obtained by a force minimization. The distances are summarized in Tab. 1. In NiS_2 , the S_2 distance is found to be about 2.1 \AA , slightly (2 %) larger than the with experimental data $d = 2.07$ [11,8]. Applying moderate pressure, the dimer decreases only slightly from 2.104 to 2.095 , thus the dimer-distance is changed by 0.4% when changing the lattice constant by 3.5%. Applying even more pressure, corresponding to a 20% volume effect, it decreases only to 2.07 \AA . Also when expanding the volume drastically, the dimer-distance vary hardly, compare [14]. For this reason, the metal-insulator transition applying pressure is related to a volume effect, since the dimer-distance is nearly less constant when varying the volume. Turning to the doped samples, we find a large variation of the dimer-distances with doping. In NiSe_2 , the Se-Se distance is given by $d = 2.49 \text{ \AA}$, which is about 4% larger than the experimental [11]. Worth mentioning is that the Se-Se distance is larger than the Ni-Se distance. Turning to NiSSe , we observe that in NiSSe I the the S-S/Se-Se distances are comparable to dimer-distances of the pristine materials, see Tab. reftab. In NiSSe II , on the other hand, the S-Se distance corresponds to the averaged value of $d=2.3\text{\AA}$.

Table 1. Lattice constants and typical bond lengths – given in Å – of the systems under consideration, NiS_2 , compressed NiS_2 , expanded NiS_2 , NiSSe , and NiSe_2 . In addition, the energy differences of the bonding and anti-bonding splitting of the chalcogen (S, Se) s and p states are given.

System	a (Å)	d : Ni–S/Se	d : S(e)–S(e)
NiS_2	5.28	2.21	2.07
NiS_2	5.49	2.31	2.10
NiS_2	5.69 (exp.)	2.40	2.10
NiS_2	6.04	2.56	2.11
NiSSe I	5.87	2.48 (S)	2.14
		2.44 (Se)	2.42
NiSSe II	5.87	2.41 (S)	2.30
		2.50 (Se)	
NiSe_2	5.96	2.48	2.49

System	a (Å)	ΔE_s (eV)	ΔE_p (eV)
NiS_2	5.28	2.2	11.0
NiS_2	5.49	3.2	9.9
NiS_2	5.69 (exp.)	3.4	9.0
NiS_2	6.04	2.3	7.2
NiSSe I	5.87	3.35 (S)	8.6 (S)
		2.3 (Se)	8.0 (Se)
NiSSe II	5.87	1.9	7.7
NiSe_2	5.96	1.8	7.4

Next, we study the volume/dimer-distance effect on the electronic structure, see Fig. 1, where we show the density of states (DOS) of NiS_2 . Generally, the presence of S/Se₂ dimers in the pyrites leads to a splitting of the bonding and anti-bonding S 3s states as well as S 3p states,

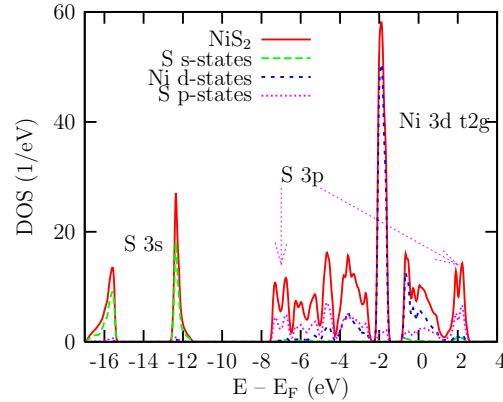


Fig. 1. (Color online) Density of states of NiS_2 . We show the S 3s, S 3p, and Ni 3d states. The bonding and antibonding parts of the S 3p states are indicated.

as indicated. A change of the volume is expected to modify the bandwidth. With increasing volume the bandwidth should decrease, and vice versa. However, the situation in NiS_2 is more complicated as pointed out for FeS_2 in [12]. Following the detailed analysis in [12] the peaks at -16 and -12 eV are assigned to S 3s states. These states are observed in the XPS valence spectra at -15 and -11 eV [6]. Thus, the splitting is correctly described in GGA, but the position shifted by 1 eV. Dominant S 3p contributions are found at the lower band edge (at -7 eV) and the upper band edge (at 2 eV). They form in itself a double peak structure, compare [12]. The Ni 3d e_g states – located between -4.5 eV and -2.54 eV and between -1 eV to 1 eV – overlap with S 3p states. The Ni 3d t_{2g} states, located at -2 eV, show almost no overlap with the S 3p-states.

Applying pressure, see Fig. 2, upper panel, where we show a comparison of the DOS of compressed and uncompressed NiS_2 , a rigid shift of the t_{2g} by -0.5 eV due to the enhanced crystal field splitting is observed in the

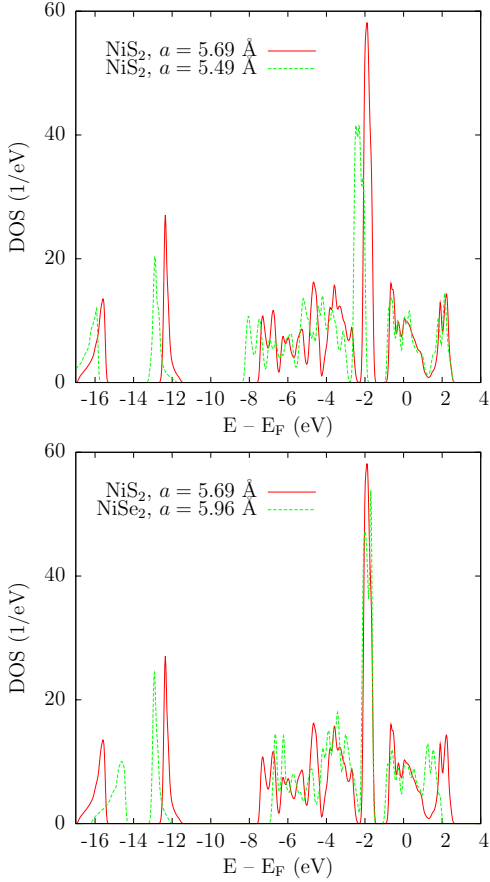


Fig. 2. (Color online) Upper panel: Density of states of NiS_2 at the experimental lattice constant and compressed NiS_2 . The straight (red) line corresponds to zero pressure, the dotted (green) line to 12 GPa. Lower panel: Density of states of NiS_2 (red line) in comparison to the density of states of NiSe_2 (green line).

DOS. Due to this shift the Ni t_{2g} - and the S p -states overlap. The states below -3 eV are subject to an additional shift, so that the lower band edge is about 0.6 eV lower for $a = 5.49$ Å than for $a = 5.69$ Å. Hence the overall band width is broader and the bonding anti-bonding splitting increases when compressing the lattice. In addition to the shift, the binding S $3p$ -states show a slight broadening, but the rigid band shift is the dominant effect.

Upon doping, see Fig. 2, lower panel, where we show a comparison of the DOS of NiS_2 and NiSe_2 , the bonding-antibonding splitting is reduced due to the increased Se-Se distance, both for the s and p states, see Tab. 1, as compared to NiS_2 . In NiSSe I , the low energy double peak structure due to the s states splits into four peaks due to the presence of both S-S and Se-Se dimers with different dimer lengths. This could be an experimental signature whether a structure with both S-S and Se-Se dimers is realized or only S-Se pairs are present. The dip at E_F is more pronounced in the NiSSe II than in the NiSSe I structure. In addition, the conduction band width is smaller in structure II (taken at the same volume). To summarize, the dominant effect of doping on the DOS/band width is the decrease of the splitting of the S $3p$ -states and the resulting stronger overlap of the Ni $3d$ with the S p states, as commonly suggested. The stronger hybridization is identified as the driving mechanism of the metal-insulator transition upon doping.

Up to now, we have analyzed the density of states over the whole band width. Turning to the underlying band structure, we take closer look at the states near the Fermi level. Interestingly, the changes in the dispersion $\epsilon(k)$ around E_F are similar when applying pressure and with doping. For comparison, we plot the according band structures in Fig. 3. The changes in the band structure near the Fermi level with pressure can be focused on two symmetry points: The band at Γ (0.3 eV) moves downwards, almost touching or crossing the Fermi level, respectively. Second, the four degenerate bands at M are shifted

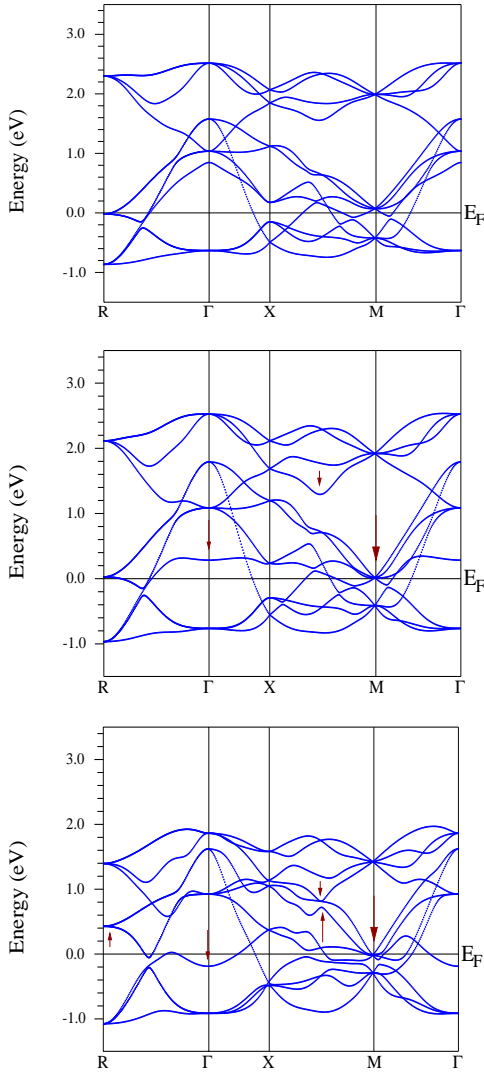


Fig. 3. (Color online) Band structure near E_F of – from top to bottom – NiS_2 , NiS_2 with 10% volume reduction and for NiSe_2 .

towards the Fermi level. In NiSe_2 , the band at R moves from the Fermi level to about 0.4 eV above. The hybridization due to band shifts or decreased bonding-antibonding splitting does not manifest itself near E_F .

3 Magnetic phase diagram

The phase boundaries of the AFM ordering of type I with pressure and doping can be reproduced within the DFT calculations using GGA. From the experience with LDA/GGA studies of other magnetic materials it is expected that LDA underestimates and GGA overestimates magnetic order and magnetic moments, see for example [25]. In NiS_2 , we consider an antiferromagnetic alignment of type A, i. e. the magnetic structure consists of ferromagnetic planes which are coupled antiferromagnetically. Using this structure no supercell is needed, in accordance with [3]. The magnetic properties – calculated within GGA – are summarized in Tab. 2. The given magnetic structure is stable within the GGA calculations, frustration effects play a minor role. As expected, NiS_2 turns out to be a high-spin compound with $\mu = 0.73\mu_B$. With increasing pressure, the magnetic moment as well as the energy difference to the non-magnetic case decreases. Increasing the pressure up to 12 GPa, the antiferromagnetic ground state is still favored, but the energy difference to the non-magnetic solution tends to zero. NiSe_2 turns out to be non-magnetic, with zero moment. At the critical doping (NiSSe), we find also an antiferromagnetic order, which can be suppressed by applying pressure. Unfortunately, a lower boundary of the magnetic transition by using LDA could not be determined since LDA favors the non-magnetic solution in all cases. This can be related to a volume effect. Within LDA the ground state volumes are much smaller than the experimental or GGA volumes which may have an impact on the spin-polarized calcula-

tions. For completeness, the data for the energy differences using LDA are also given in Tab. 2.

The electronic properties change due to the magnetic order. Band structure and density of states are heavily influenced by the magnetism, see Fig. 4, where we show DOS and band structure of antiferromagnetic NiS₂. The degeneracy of the bands is lifted from a fourfold to a twofold degeneracy. States near E_F, especially at R and M, are emptied. As a result, the dip in the DOS at the Fermi level becomes more pronounced.

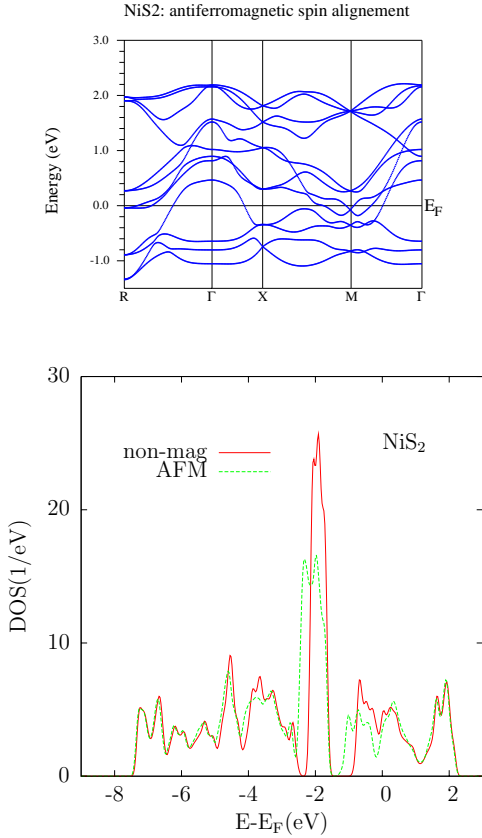


Fig. 4. (Color online) Band structure and density of states of NiS₂ with anti-ferromagnetic spin configuration.

Table 2. Magnetic ground state and magnetic moment (in μ_B) within LDA/GGA calculations for the systems under investigation. $\Delta E = (E_{\text{non-pol}} - E_{\text{mag}})/(\text{number of Ni})$ is the energy gain due to the magnetic ordering per Ni atom and is given in meV.

compound	V _{xc}	mag. moment	ΔE
NiS ₂ , 5.69 Å	GGA	± 0.73	2.1
NiS ₂ , 5.69 Å	LDA	± 0.20	-0.14
NiS ₂ , 5.49 Å	GGA	± 0.45	0.17
NiS ₂ , 5.49 Å	LDA	± 0.11	-0.17
NiS ₂ , 5.28 Å	GGA	0	-
NiSSe, 5.69	GGA	± 0.4	0.034
NiSSe, 5.87	GGA	$\pm 0.5 - \pm 0.6$	0.88
NiSSe, 5.87	LDA	± 0.15	-0.14
NiSe ₂ , 5.96	GGA	0	-

4 GGA+U, Fock exchange

Local approximations to DFT like LDA and GGA fail to describe the insulator [13]. Recently, a variety of insulating transition-metal oxides have been investigated using LDA+U [17], LDA+DMFT [14], Fock exchange or hybrid functionals [19], or the *GW* approximation [26]. In this work, we apply GGA+U, hybrid functionals, Hartree-Fock, and *GW* calculations to NiS₂. We use the implementation of GGA+U, comparing the fully localized limit (SIC) as applied to NiO [17] and the around mean-field treatment (AFM) [27] for the double counting correction, and the EECE treatment [19] within the wien2k code [15].

To start with, we perform constraint GGA calculation to obtain a reasonable value for *U*. Following the treatment in [28] and assuming a Ni d⁸ configuration as in

NiO , we obtain $U_{\text{eff}} = U - J = 6.39$ eV for NiS_2 . U_{eff} decreases to 5.89 eV for NiSSe , and further to 4.94 eV for NiSe_2 . The different chemistry such leads to a considerable decrease of the correlation energy with doping. With decreasing volume, U_{eff} is constant. In the following, we always use the antiferromagnetic spin structure as discussed in the previous section. The DOS, calculated with $U_{\text{eff}} = 6.4$ eV and the SIC correction, is plotted in Fig. 5, upper panel, and shows a rather poor agreement with experimental data [6,7]. The Ni 3d states are shifted to too low energies, forming a triple peak structure at the lower band edge. The S 3p states are homogeneously spread over the whole energy range. Using the experimental value of $U = 5$ eV the gap values, namely $\Delta^{\text{SIC}} = 0.6$ eV and $\Delta^{\text{AFM}} = 0.3$ eV, are in the range of the experimental values, but the Ni 3d states are located at -4 eV instead of -2 eV. A similar behavior was found in case of the ferromagnetic metallic pyrite CoS_2 [29].

While $\text{GGA}+U$ is successful for insulators, the description of correlated metals where the requirement of an integer orbital occupation and well established long range order [30] is no longer fulfilled may fail. In case of NiS_2 under pressure, $\text{GGA}+U$ correctly shows that this system is a non-magnetic metal. The results for NiSe_2 on the other hand, are very sensitive to the choice of the method. Using SIC the ground state is a ferromagnetic metal, in case of AFM the antiferromagnetic metal is nearly degenerate to a ferromagnetic metal with two different moments.

In a next step we perform calculation using Fock exchange for the Ni within the muffin tin spheres (exact ex-

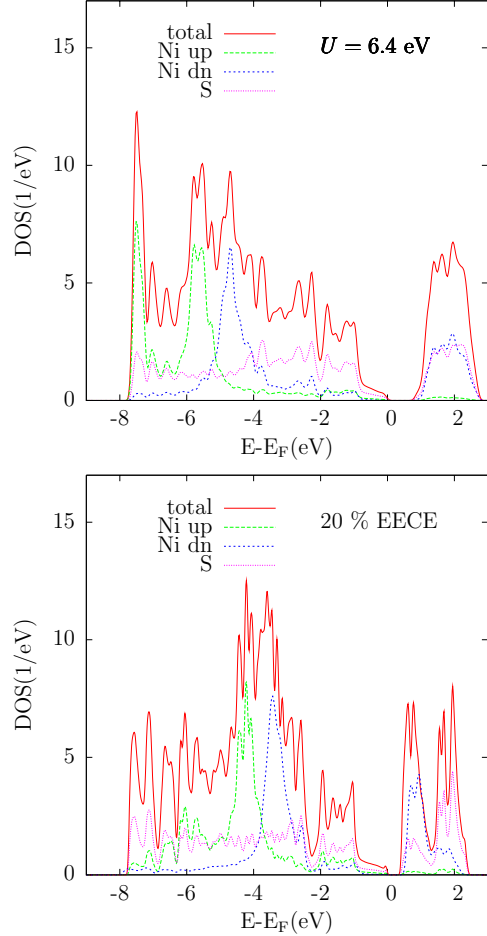


Fig. 5. (Color online) Total density of states of NiS_2 (red line) and contributions of the Ni 3d (green and blue line) and S 3p (pink line) orbitals: we compare the $\text{GGA}+U$ calculation (left-hand side) with the hybrid functional with 20% EECE (right-hand side).

change for correlated electrons, EECE) and LDA for the correlation potential. This approach is known to give quite reasonable results for correlated electron systems [18,19]. Instead of a parameter U and the choice for the double counting corrections which give deviating results for insulating NiS_2 and metallic NiSe_2 , the mixing parameter of the hybrid functional has to be determined. As expected 100 % EECE overestimates the gap by a factor of 5. It

also shifts the Ni $3d$ states to the lower band edge, i. e. to -10 to -8 eV. In this way, 100 % EECE is comparable to $U = 10.7$ eV. The gap is induced within the S p states, and not as expected between the Ni $3d$ (Mott-Hubbard type) or Ni $3d$ and S $3p$ states (charge transfer type). If 25 % EECE is added to LDA the Ni $3d_{t2g}$ states are found at -4 eV. The DOS shape corresponds to the DOS obtained for $U = 5.4$ eV (suggested U value from [11]). Decreasing the amount of EECE further, the gap closes below 20%; therefore we perform the following calculation with a hybrid functional where 20% EECE is mixed to LDA. Then, gap in the DOS opens within the Ni-S hybridized states, located between -2 and 1 eV, at the preformed dip in the GGA calculation, as can be seen in Fig. 5. The bonding-antibonding S $3p$ states dominate at the lower valence and higher conduction band edge. The double peak structure of the empty states observed in XAS can be traced back to a Ni $3d_{eg}$ double peak and the S $3p$ antibonding double peak. Using this hybrid functional, an antiferromagnetic solution is obtained, although LDA itself favors the non-magnetic ground state. The calculated moments become smaller under pressure and with doping but do not vanish.

The gap of NiS₂ is very sensitive to the S-S dimer-distance d . Using a structure with $d = 2.15$ Å the band gap amounts to 0.3 eV, whereas it is 0.6 eV with $d = 2.10$ Å. Increasing the dimer distance to $d = 2.36$ Å, i.e. using the structural parameter of NiSe₂ but the lattice constant of NiS₂, the gap closes. A closer look at the weighted band structure shows that the gap is located at Γ ; the lower band has dominant Ni character, whereas the upper

band has dominant S character. The S character of this band shows up only at Γ , compare FeS₂ [12]. According to the band structure the metal-insulator transition under pressure is triggered by the band with Ni character which provides the states at the Fermi level between Γ and X. With doping the metallic state is attributed to the states between X and M. In this way, a metallic ground state is obtained for NiSe₂ due to the increased dimer-distance. On the other hand, reducing the volume also closes the gap at constant dimer-distance. The results for the band structure are shown in Fig. 6, where we compare insulating NiS₂ with metallic NiS₂ under pressure and metallic NiSe₂.

To summarize, GGA+ U is not able to describe the system properly, neither with the calculated nor estimated U values. Hybrid functionals using Fock exchange can reproduce the insulator and give a reasonable DOS. This approach fails, however, in describing the magnetic phase diagram by overestimating the ordered phase. Thus, we have identified a system where the advantage of hybrid functionals versus GGA+ U can be clearly demonstrated.

5 Quasi-particle picture: HF and GW

Corrections to the energy eigenvalues in DFT can be estimated by first order many-body perturbation theory with respect to the difference in exchange correlation self-energy and exchange correlation potential of DFT. Describing the dielectric properties of semiconductors, the GW approximation has become the method of choice [31]. Thereby, the non-local, energy-dependent self-energy is approximated

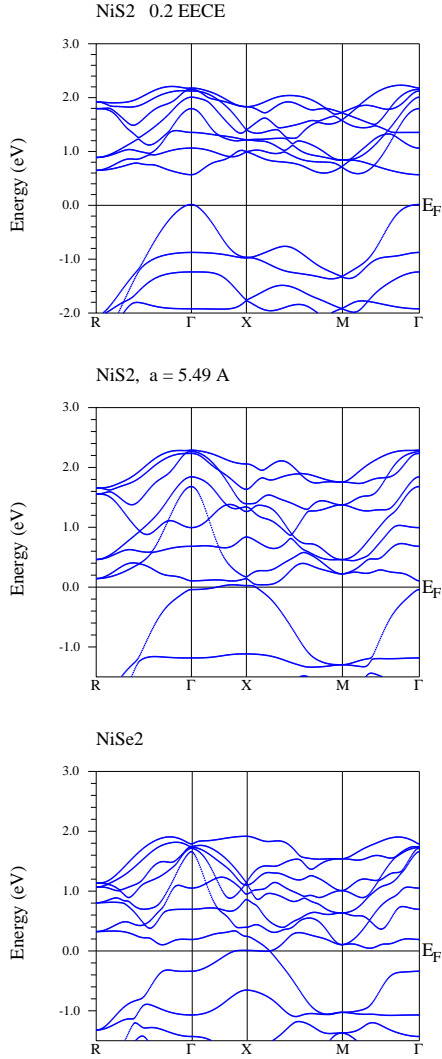


Fig. 6. Band structure obtained using a hybrid functional with 20% EECE. Top: NiS_2 ; middle: NiS_2 under pressure; bottom: NiSe_2 .

by the Green's function and the screened Coulomb interaction, $\Sigma = GW$ [32]. The screening is calculated on the level of the random phase approximation. Within the “one-shot” procedure G_0 and W_0 are calculated from LDA/GGA, but this G_0W_0 approach gives appropriate results only if GW is a small correction to LDA. Transition-metal oxides can be treated rather well using self-consistent approaches. For example, the electronic structure of VO_2

is described correctly [26]. Even properties of V_2O_3 can be described [33]. In NiS_2 , the electron-lattice coupling is strong and found to be the driving mechanism of the metal-insulator transition, thus it can be expected that the GW approach is able to provide a description of the insulating state. Similar to VO_2 , in the case of NiS_2 , a self-consistent scheme has to be applied to get rid of the metallic starting point. In the following we use the GW implementation of the ABINIT package [21]. We compare, see [34], Hartree-Fock calculations with self-consistent, but static GW schemes. The self-energy can be written as a sum of the exchange self-energy (static screened exchange), the correlation self-energy (Coulomb-hole term) and the dynamical (energy-dependent) self-energy, and the approximations used within GW are classified along this partitioning. Here, we compare the screened exchange with the screened exchange plus Coulomb-hole. Another static GW approximation is the quasi-particle self-consistent GW [35]. As we start from the Kohn-Sham orbitals obtained within LDA, spin-polarized calculations are in accordance with non-polarized calculations since LDA favors a non-magnetic ground state. For simplicity we chose the k-points where the corrections are calculated out of the optimal k-set. The given k-points K1 (1/8,1/8,1/8) and K4 (3/8,3/8,3/8) are located between Γ and R, and K2 (3/8,1/8,1/8) and K3 (3/8,3/8,1/8) between X and M. As it can be assumed that the correction do not vary in the vicinity of the chosen k-points, K1 should give the correction at Γ , K2 at X, K3 at M, and K4 at R.

Table 3. Energy gaps obtained within different approximation used for the self consistency, namely screened exchange, screened exchange plus Coulomb hole, and model GW [35].

method	spin	k-point	gap
HF	non-pol	Γ	0.3 eV
HF	pol	Γ	0.4 eV
scrEX	pol	M	0.175 eV
COHSEX	non-pol	M	0.021 eV
COHSEX	pol	M	0.025 eV
QPscGW	pol	M	0.027 eV

On all GW levels, gaps are induced to the band structure of NiS_2 at the chosen k-points, where the smallest gap occurs at K3 (M). The results are summarized in Tab. 3.

The behavior is in accordance with the GGA calculations as we can assign the dip at E_F of the GGA DOS to the bands crossing at M. However, it is found that one band crosses the Fermi level between R and Γ . For this reason, GW calculations cannot describe the insulating state of NiS_2 , even though a gap is formed at all given k-points. Therefore, calculations of compressed NiS_2 and NiSe_2 lead to very similar results for the gaps. Moreover, the metallic phases show larger gaps at these k-points, but the crossing is present in each case.

On the other hand, the smallest gap is located at Γ within Hartree-Fock, in accordance with the results discussed in the previous section. In addition, the gap values resulting from the calculations with 20 % EECE and from the Hartree-Fock calculation are astonishingly of similar magnitude. However, the total density of states shows no

gap at E_F but a large gap between -5 to -1 eV, despite the direct gaps at the chosen k -points.

As a major shortcoming, the GW and Hartree-Fock calculations, on top of the non-magnetic starting point generated by the LDA, do not generate a magnetic ground state as the EECE does. The local magnetic minimum is thus not obtained.

6 Summary

In summary, the electronic and magnetic structure of doped and compressed NiS_2 was discussed in great detail within different approximation in the framework of DFT. In particular, LDA/GGA, GGA+ U , and a hybrid functional composed of 20% EECE mixed to LDA have been compared to Hartree-Fock and GW calculations. The metal-insulator transition with applying pressure or doping in NiS_2 can be described properly only when using the hybrid functional. The GGA+ U fails to describe correlated metals since it works only well in case of integer orbital occupation and long range order. However, as the electron-lattice interaction is very strong in NiS_2 , and the results very sensitive to changes in the lattice structure, the results of LDA/GGA calculations already allows to identify the microscopic origin of the metal-insulator transition, namely the dependence on crystal field splitting and bonding-antibonding splitting. Additional corrections to LDA/GGA are then necessary to provide the insulating band structure of NiS_2 .

Therefore, the magnetic properties of NiS_2 , on the other hand, are described best within GGA. LDA under-

estimates the magnetic order, thus no magnetic ground state is found. The employed hybrid functional overestimates the magnetic order, even when only a small amount of Fock exchange is mixed to LDA. The GGA+ U approach cannot capture the magnetic properties as expected for metallic compounds away from half band filling.

Thus, the Fock exchange applied to the transition metal Ni in the EECE approach gives reasonable results as compared to experimental data as far as the electronic properties are concerned as well as in the insulating as the metallic phases of NiS_2 . The ordering of the magnetic moments is highly overestimated. The magnetic order present in the EECE approach alters the band structure in comparison to Hartree-Fock.

7 Acknowledgements

We acknowledge fruitful discussions with L. Baldassarre, U. Eckern, V. Eyert, M. Gatti, and J. Kuneš. Some of the presented results have been obtained through the use of the ABINIT code, a common project of the Université Catholique de Louvain, Corning Incorporated, and other contributors (URL <http://www.abinit.org>). The pseudopotentials were provided by S. Botti and M. Gatti. Financial support was provided by the Deutsche Forschungsgemeinschaft (SFB 484)

References

1. F. Gautier, G. Krill, M. F. Lapiere, P. Panissod, C. Robert, G. Czjzek, J. Fink, and H. Schmidt, *Phys. Lett.* **53A**, 31 (1975)
2. J. A. Wilson and G. D. Pitt, *Phil. Mag.* **23**, 1297 (1971)
3. Y. Sekine, H. Takahashi, N. Mōri, T. Matsumoto, and T. Kosaka, *Physica B: Condensed Matter* **237-238**, 148 (1997)
4. R. L. Kautz, M. S. Dresselhaus, D. Adler, and A. Linz, *Phys. Rev. B* **6**, 2078 (1972)
5. A. Y. Matsuura, Z.-X. Shen, D. S. Dessau, C.-H. Park, T. Thio, J. W. Bennett, and O. Jepsen, *Phys. Rev. B* **53**, R7584 (1996)
6. L. Sangaletti, F. Parmigiani, T. Thio, and J. W. Bennett, *Phys. Rev. B* **55**, 9514 (1997)
7. K. Mamiya *et. al.*, *Phys. Rev. B* **58**, 9611 (1998)
8. S. R. Krishnakumar and D. D. Sarma, *Phys. Rev. B* **68**, 155110 (2003)
9. D. D. Sarma, S. R. Krishnakumar, E. Weschke, C. Schüffler-Langeheine, C. Mazumdar, L. Kilian, G. Kaindl, K. Mamiya, S.-I. Fujimori, A. Fujimori, and T. Miyadai, *Phys. Rev. B* **67**, 155112 (2003)
10. J. M. Tomczak and S. Biermann, *J. Phys.: Condens. Matter* **21**, 064209 (2009)
11. W. Folkerts, G. A. Sawatzky, C. Haas, R. A. de Groot, and H. U. Hillebrecht, *J. Phys. C* **20**, 4135 (1987)
12. V. Eyert, K.-H. Höck, S. Fiechter, and H. Tributsch, *Phys. Rev. B* **57**, 6350 (1998)
13. A. Perucchi, C. Marini, M. Valentini, P. Postorino, R. Sopracase, P. Dore, P. Hansmann, O. Jepsen, G. Sangiovanni, A. Toschi, K. Held, D. Topwal, D. D. Sarma, and S. Lupi, *Phys. Rev. B* **80**, 073101 (2009)
14. J. Kuneš, L. Baldassarre, B. Schachner, C. A. Kuntscher, Dm. M. Korotin, V. I. Anisimov, arXiv:0907.2154

15. P. Blaha, K. Schwarz, G. Madsen, D. Kvasnicka, and J. Luitz, *Wien2k: An augmented plane wave + local orbitals program for calculating crystal properties*, Vienna University of Technology, 2001.
16. J. P. Perdew, K. Burke, and M. Ernzerhof, *Phys. Rev. Lett.* **77**, 3865 (1996)
17. V. I. Anisimov, I. V. Solovyev, M. A. Korotin, M. T. Czyzyk, and G. A. Sawatzky, *Phys. Rev. B* **48**, 16929 (1993); V. I. Anisimov, D. Bukhvalov, and T. M. Rice, *Phys. Rev. B* **59**, 7901 (1999)
18. P. Novák, J. Kuneš, L. Chaput, and W. E. Pickett, *phys. stat. sol. (b)* **243**, 563 (2006)
19. F. Tran, P. Blaha, K. Schwarz, *Phys. Rev. B* **74**, 155108 (2006)
20. X. Gonze, J.M. Beuken, R. Caracas, F. Detraux, M. Fuchs, G.M. Rignanese, L. Sindic, M. Verstraete, G. Zerah, F. Jollet, M. Torrent, A. Roy, M. Mikami, Ph. Ghosez, J.Y. Raty, and D.Č. Allan, *Comp. Mat. Sci.* **25**, 478 (2002)
21. X. Gonze, G.M. Rignanese, M. Verstraete, J.M. Beuken, Y. Pouillon, R. Caracas, F. Jollet, M. Torrent, G. Zerah, M. Mikami, Ph. Ghosez, M. Veithen, J.Y. Raty, V. Olevano, F. Bruneval, L. Reining, R. Godby, G. Onida, D.Ř. Hamann, and D.Č. Allan, *Zeit. Kristallogr.* **220**, 558 (2005)
22. T. A. Bither, R. J. Bouchard, W. H. Cloud, P. C. Donohue, and W. J. Siemons, *Inorg. Chem.* **7**, 2208 (1968)
23. K. Iwaya, Y. Kohsaka, S. Satow, T. Hanaguri, S. Miyasaka, and H. Takagi, *Phys. Rev. B* **70**, 161103 (2004)
24. P. Kwizera, M. S. Dresselhaus, and D. Adler, *Phys. Rev. B* **21**, 2328 (1980)
25. R. Hafner, D. Spisk, R. Lorenz, and J. Hafner, *J. Phys.: Condens. Matter* **13**, L239 (2001)
26. M. Gatti, F. Bruneval, V. Olevano, and L. Reining, *Phys. Rev. Lett.* **99**, 266402 (2007)
27. M. T. Czyzyk and G. A. Sawatzky, *Phys. Rev. B* **49**, 14211 (1994)
28. G. K. H. Madsen and P. Novák, *EPL* **69**, 77 (2005)
29. S. K. Kwon, S. J. Youn, and B. I. Min, *Phys. Rev. B* **62**, 357 (2000)
30. I. S. Elfimov, G. A. Sawatzky, A. Damascelli, *Phys. Rev. B* **77**, 060504(R) (2008)
31. W. G. Aulbur, L. Jönsson, and J. Wilkins, in *Solid State Physics*, edited by H. Ehrenreich and F. Saepen (Academic Press, New York, 2000), Vol. 54, p. 1
32. L. Hedin, *Phys. Rev.* **139**, A796 (1965)
33. E. Papalazarou, M. Gatti, M. Marsi, V. Brouet, F. Iori, L. Reining, E. Annese, I. Vobornik, F. Offi, A. Fondacaro, S. Huotari, P. Lacovig, O. Tjernberg, N. B. Brookes, M. Sacchi, P. Metcalf, and G. Panaccione, arXiv:0903.4303
34. F. Bruneval, N. Vast, and L. Reining, *Phys. Rev. B* **74**, 045102 (2006), 045102
35. S. V. Faleev, M. van Schilfgaarde, and T. Kotani, *Phys. Rev. Lett.* **93**, 126406 (2004)

Electronic and magnetic properties of $\text{NiS}_{2-x}\text{Se}_x$: a comparative study

Cosima Schuster

Institut für Physik, Universität Augsburg, 86135 Augsburg, Germany

(Dated: October 30, 2018)

The metal-insulator transition and the problem of d -electron delocalization are investigated in the pyrite system $\text{NiS}_{2-x}\text{Se}_x$ under pressure using density functional theory (DFT). We test several approximations, including the generalized gradient approximation (GGA), the GGA+ U approach, and hybrid functionals. In addition we apply the GW approximation and perform Hartree-Fock calculations. The important role of the chalcogen dimers in the electronic structure is discussed within GGA, which sufficiently describes the role of the lattice in the metal-insulator transition. In addition, the magnetic phase diagram is determined. However, the electronic properties are inadequately described – the insulating ground state of NiS_2 cannot be obtained – and the magnetic order is slightly overestimated. If correlations are taken into account within GGA+ U , the insulator is found, but the non-magnetic ground state of the doped samples is not accessible. Mixing Fock exchange with local approximations as GGA correctly reproduce the insulating ground state in NiS_2 , and metallic ground states with doping and pressure. The insulator is – in contrast to earlier suggestions – of Mott type, i. e. the gap opens between Ni $3de_g$ states. Due to the Fock term, the magnetic order is strongly overestimated. The applied GW calculations are not able to correct the metallic character of NiS_2 and underestimate the gap by one order of magnitude.

PACS numbers: 73.20.-r, 74.25.Jb, 85.25.Am

Keywords: Metal-insulator transition, density functional theory, magnetic phase diagram

I. INTRODUCTION

Crystal field splitting, electron-electron interaction, and the $3d$ band width are almost equal in the pyrites MX_2 ($M=\text{Fe, Co, Ni, Cu, Zn}$; $X=\text{S, Se}$) which gives rise to a large variety of electrical, magnetic and optical properties in these compounds. Of special interest is the metal-insulator transition in NiS_2 with Se-doping [1] or under pressure [2]. The transition is not accompanied by a change in the lattice symmetry and is commonly believed to be driven by the electron-electron interaction. In addition, a low-temperature antiferromagnetic phase is observed both in the insulating and metallic regime of $\text{NiS}_{2-x}\text{Se}_x$ [1] and by applying pressure in NiS_2 [3]. The electronic and optical properties of NiS_2 were first investigated already 30 years ago [4], and re-investigated experimentally in the late nineties [5, 6, 7, 8, 9]. The renewed interest in transition-metal oxides and their metal-insulator transitions traces back to the attempt to understand the phase diagram of the high- T_c superconducting perovskites. Moreover, the attempt to use the metal-insulator transition of V_2O_3 or VO_2 for technical applications triggered many studies up to now [10].

Theoretical attempts using density functional theory and the local density approximation (LDA) to describe the electronic structure of the pyrites date back to 1987 [11], with the focus on FeS_2 , where the important role of the S(e)-S(e) dimers present in the pyrite structure has been pointed out. The role of electron-lattice interaction when applying pressure was studied ten years later, again in FeS_2 [12]. Other pyrites are mentioned in [11], and their electronic structure is explained by filling the band structure with the d -electrons of the transition metal by going from Fe ($3d^6 4s^2$) to Zn ($3d^{10} 4s^2$). The band insulators are described quite well within the local density ap-

proximation. however the microscopic origin of the insulating nature of NiS_2 is not well understood. Since more advanced approximations within DFT are available now, several attempts to improve the material specific theory have been performed. Recently, Perucchi *et al.* [13] have discussed two different mechanism for the metal-insulator transitions based on LDA calculations. Compression and expansion of the lattice alter the metallic state, albeit through two different microscopic mechanisms. On the other hand, Kuneš *et al.* [14], using LDA+DMFT, have traced back the metal-insulator transition to a single control parameter, namely the size of the p gap. They confirmed, however, that compression and doping influences this control parameter in different ways. Both studies concentrate on the electronic structure in the paramagnetic phase and neglect the magnetism.

Hence, we clarify the role of the S-S dimers and discuss the energy scales mentioned in [13, 14]. For the calculations we use the wien2k code [15] and the generalized gradient approximation (GGA) in the parameterization of PBE [16]. In a next step we determine the magnetic phase diagram, Sec. III. Surprisingly, GGA describes the magnetic phase diagram quite well, slightly overestimating the phase boundaries as compared to experimental data. In contrast to GGA, LDA always favors the non-magnetic ground state. Calculations using improved exchange-correlations functionals are presented in Sec. IV. We present results of GGA+ U (SIC) [17] and EECE hybrid [18, 19] calculations. To compare with we have performed also GW calculations on top of LDA using ABINIT [20, 21]. We focus on the advantages and shortcomings of the different techniques with regard to correlated materials.

II. THE ROLE OF THE DIMERS FOR THE ELECTRONIC STRUCTURE

The pyrite structure is a simple cubic lattice with space group $\text{Pa}\bar{3}$. It is best described in terms of the NaCl structure with the transition metal in one sub-lattice and the center of mass of the chalcogenide pairs in the other. Thus, the S/Se atoms form distorted octahedra around the Ni atoms. In the following, we use the experimental lattice constant of NiS_2 , $a = 5.687 \text{ \AA}$ [22]. Applying hydrostatic pressure is simulated by a shortening of the lattice constant – 5%/10% volume reduction correspond to 1.7%/3.5% reduction of the lattice constant and to 5/12 GPa, respectively. In the attempt to understand the phase diagram with doping we concentrate on the end points with $x = 0$ and $x = 2$. In addition we consider also $x = 1$, i. e. NiSSe . For NiSe_2 we also use the experimental lattice constant, $a = 5.960 \text{ \AA}$ [22]. In case of NiSSe , we study two different configurations within the pyrite unit cell – recent STM measurement on doped samples show no sign of a superstructure [23] – and use the theoretically obtained volume, $a_{\text{theo}} = 5.87 \text{ \AA}$ which is about 1% larger than estimated in experiments [1, 24]. The first configuration contains S_2 and Se_2 dimers, the second only S–Se pairs. Thereby the second configuration is favored by 0.015 Ryd when the volume is fixed. In general, S–S, S–Se, and Se–Se pairs are present in doped samples [8].

Using the mentioned lattice constants the internal positions are obtained by a force minimization. The distances are summarized in Tab. I. In NiS_2 , the S_2 distance is found to be about 2.1 Å, slightly (2%) larger than the with experimental data $d = 2.07$ [8, 11]. Applying moderate pressure, the dimer decreases only slightly from 2.104 to 2.095, thus the dimer-distance is changed by 0.4% when changing the lattice constant by 3.5%. Applying even more pressure, corresponding to a 20% volume effect, it decreases only to 2.07 Å. Also when expanding the volume drastically, the dimer-distance vary hardly, compare [14]. For this reason, the metal-insulator transition applying pressure is related to a volume effect, since the dimer-distance is nearly less constant when varying the volume. Turning to the doped samples, we find a large variation of the dimer-distances with doping. In NiSe_2 , the Se–Se distance is given by $d = 2.49 \text{ \AA}$, which is about 4% larger than the experimental [11]. Worth mentioning is that the Se–Se distance is larger than the Ni–Se distance. Turning to NiSSe , we observe that in NiSSe I the the S–S/Se–Se distances are comparable to dimer-distances of the pristine materials, see Tab. reftab. In NiSSe II , on the other hand, the S–Se distance corresponds to the averaged value of $d=2.3\text{\AA}$.

Next, we study the volume/dimer-distance effect on the electronic structure, see Fig. 1, where we show the density of states (DOS) of NiS_2 . Generally, the presence of S/Se₂ dimers in the pyrites leads to a splitting of the bonding and anti-bonding S 3s states as well as S 3p states, as indicated. A change of the volume is expected

System	a (Å)	d : Ni–S/Se	d : S(e)–S(e)	ΔE_s (eV)	ΔE_p (eV)
NiS_2	5.28	2.21	2.07	2.2	11.0
NiS_2	5.49	2.31	2.10	3.2	9.9
NiS_2	5.69 (exp.)	2.40	2.10	3.4	9.0
NiS_2	6.04	2.56	2.11	2.3	7.2
NiSSe I	5.87	2.48 (S)	2.14	3.35 (S)	8.6 (S)
		2.44 (Se)	2.42	2.3 (Se)	8.0 (Se)
NiSSe II	5.87	2.41 (S)	2.30	1.9	7.7
		2.50 (Se)			
NiSe_2	5.96	2.48	2.49	1.8	7.4

TABLE I: Lattice constants and typical bond lengths – given in Å – of the systems under consideration, NiS_2 , compressed NiS_2 , expanded NiS_2 , NiSSe , and NiSe_2 . In addition, the energy differences of the bonding and anti-bonding splitting of the chalcogen (S, Se) s and p states are given.

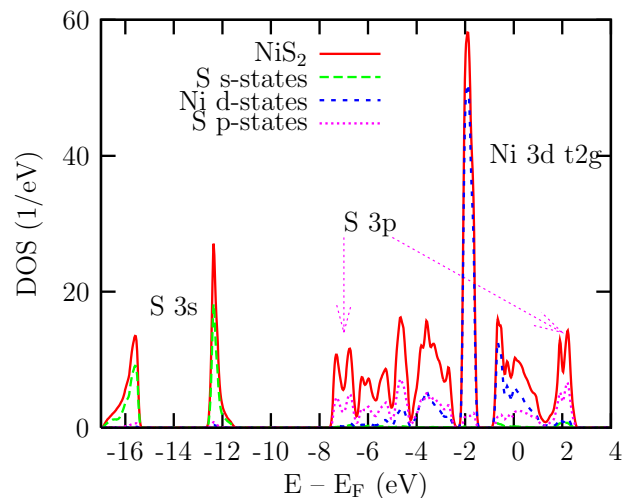


FIG. 1: (Color online) Density of states of NiS_2 . We show the S 3s, S 3p, and Ni 3d states. The bonding and antibonding parts of the S 3p states are indicated.

to modify the bandwidth. With increasing volume the bandwidth should decrease, and vice versa. However, the situation in NiS_2 is more complicated as pointed out for FeS_2 in [12]. Following the detailed analysis in [12] the peaks at -16 and -12 eV are assigned to S 3s states. These states are observed in the XPS valence spectra at -15 and -11 eV [6]. Thus, the splitting is correctly described in GGA, but the position shifted by 1 eV. Dominant S 3p contributions are found at the lower band edge (at -7 eV) and the upper band edge (at 2 eV). They form in itself a double peak structure, compare [12]. The Ni 3d e_g states – located between -4.5 eV and -2.54 eV and between -1 eV to 1 eV – overlap with S 3p states. The Ni 3d t_{2g} states, located at -2 eV, show almost no overlap with the S 3p-states.

Applying pressure, see Fig. 2, upper panel, where we show a comparison of the DOS of compressed and uncompressed NiS_2 , a rigid shift of the t_{2g} by -0.5 eV due to the enhanced crystal field splitting is observed in the DOS. Due to this shift the Ni t_{2g} - and the S p -states

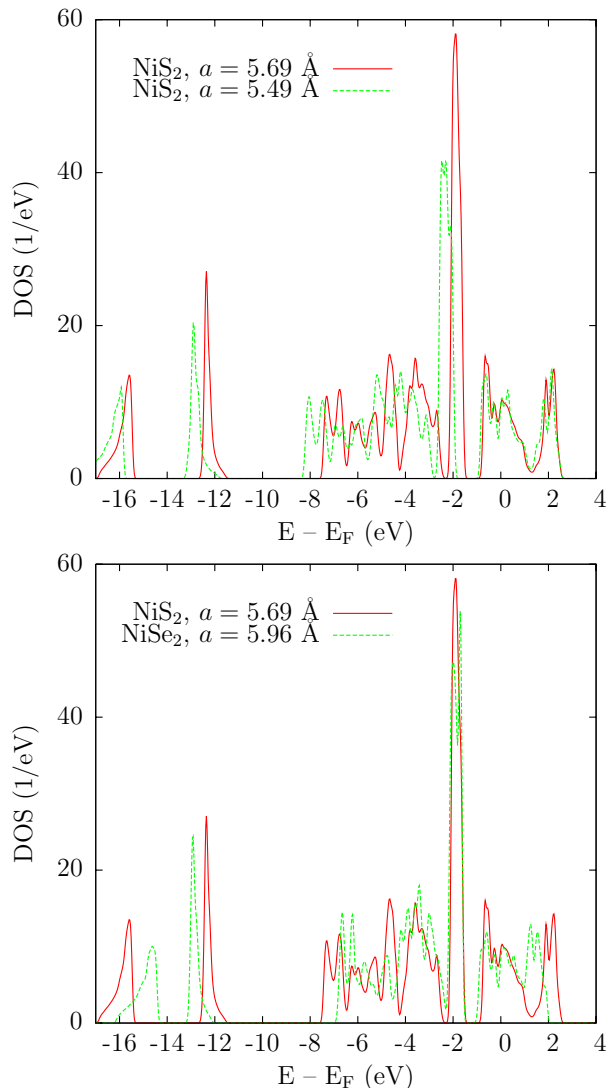


FIG. 2: (Color online) Upper panel: Density of states of NiS_2 at the experimental lattice constant and compressed NiS_2 . The straight (red) line corresponds to zero pressure, the dotted (green) line to 12 GPa. Lower panel: Density of states of NiS_2 (red line) in comparison to the density of states of NiSe_2 (green line).

overlap. The states below -3 eV are subject to an additional shift, so that the lower band edge is about 0.6 eV lower for $a = 5.49$ Å than for $a = 5.69$ Å. Hence the overall band width is broader and the bonding anti-bonding splitting increases when compressing the lattice. In addition to the shift, the binding S $3p$ -states show a slight broadening, but the rigid band shift is the dominant effect.

Upon doping, see Fig. 2, lower panel, where we show a comparison of the DOS of NiS_2 and NiSe_2 , the bonding-antibonding splitting is reduced due to the increased Se-Se distance, both for the s and p states, see Tab. I, as compared to NiS_2 . In NiSSe I, the low energy double peak structure due to the s states splits into four peaks

due to the presence of both S-S and Se-Se dimers with different dimer lengths. This could be an experimental signature whether a structure with both S-S and Se-Se dimers is realized or only S-Se pairs are present. The dip at E_F is more pronounced in the NiSSe II than in the NiSSe I structure. In addition, the conduction band width is smaller in structure II (taken at the same volume). To summarize, the dominant effect of doping on the DOS/band width is the decrease of the splitting of the S $3p$ -states and the resulting stronger overlap of the Ni $3d$ with the S p states, as commonly suggested. The stronger hybridization is identified as the driving mechanism of the metal-insulator transition upon doping.

Up to now, we have analyzed the density of states over the whole band width. Turning to the underlying band structure, we take closer look at the states near the Fermi level. Interestingly, the changes in the dispersion $\epsilon(k)$ around E_F are similar when applying pressure and with doping. For comparison, we plot the according band structures in Fig. 3. The changes in the band structure near the Fermi level with pressure can be focused on two symmetry points: The band at Γ (0.3 eV) moves downwards, almost touching or crossing the Fermi level, respectively. Second, the four degenerate bands at M are shifted towards the Fermi level. In NiSe_2 , the band at R moves from the Fermi level to about 0.4 eV above. The hybridization due to band shifts or decreased bonding-antibonding splitting does not manifest itself near E_F .

III. MAGNETIC PHASE DIAGRAM

The phase boundaries of the AFM ordering of type I with pressure and doping can be reproduced within the DFT calculations using GGA. From the experience with LDA/GGA studies of other magnetic materials it is expected that LDA underestimates and GGA overestimates magnetic order and magnetic moments, see for example [25]. In NiS_2 , we consider an antiferromagnetic alignment of type A, i. e. the magnetic structure consists of ferromagnetic planes which are coupled antiferromagnetically. Using this structure no supercell is needed, in accordance with [3]. The magnetic properties – calculated within GGA – are summarized in Tab. II. The given magnetic structure is stable within the GGA calculations, frustration effects play a minor role. As expected, NiS_2 turns out to be a high-spin compound with $\mu = 0.73\mu_B$. With increasing pressure, the magnetic moment as well as the energy difference to the non-magnetic case decreases. Increasing the pressure up to 12 GPa, the antiferromagnetic ground state is still favored, but the energy difference to the non-magnetic solution tends to zero. NiSe_2 turns out to be non-magnetic, with zero moment. At the critical doping (NiSSe), we find also an antiferromagnetic order, which can be suppressed by applying pressure. Unfortunately, a lower boundary of the magnetic transition by using LDA could not be determined since LDA favors the non-magnetic solution in all cases. This can be re-

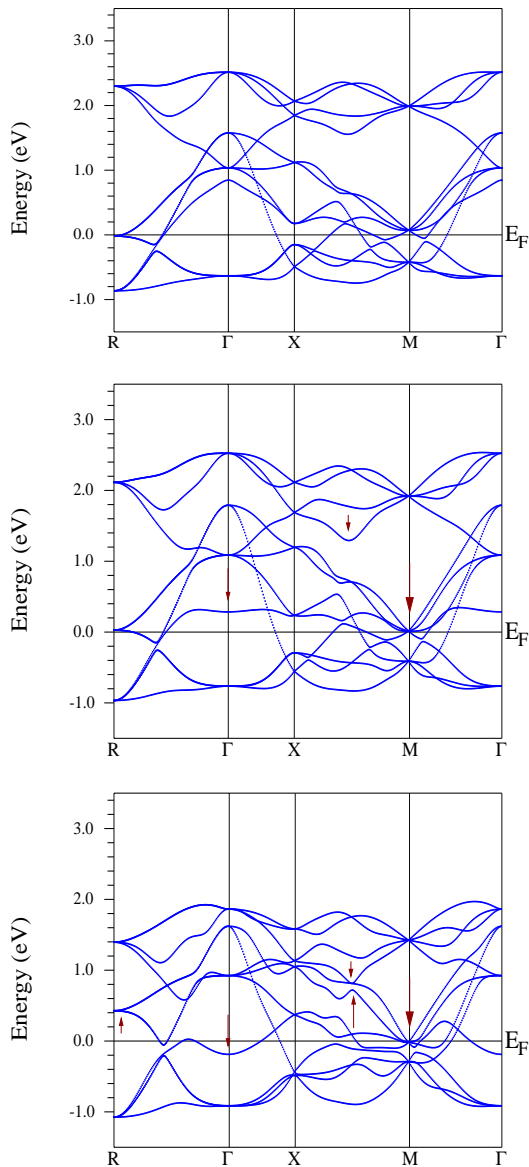


FIG. 3: (Color online) Band structure near E_F of – from top to bottom – NiS_2 , NiS_2 with 10% volume reduction and for NiSe_2 .

lated to a volume effect. Within LDA the ground state volumes are much smaller than the experimental or GGA volumes which may have an impact on the spin-polarized calculations. For completeness, the data for the energy differences using LDA are also given in Tab. II.

The electronic properties change due to the magnetic order. Band structure and density of states are heavily influenced by the magnetism, see Fig. 4, where we show DOS and band structure of antiferromagnetic NiS_2 . The degeneracy of the bands is lifted from a fourfold to a twofold degeneracy. States near E_F , especially at R and M, are emptied. As a result, the dip in the DOS at the Fermi level becomes more pronounced.

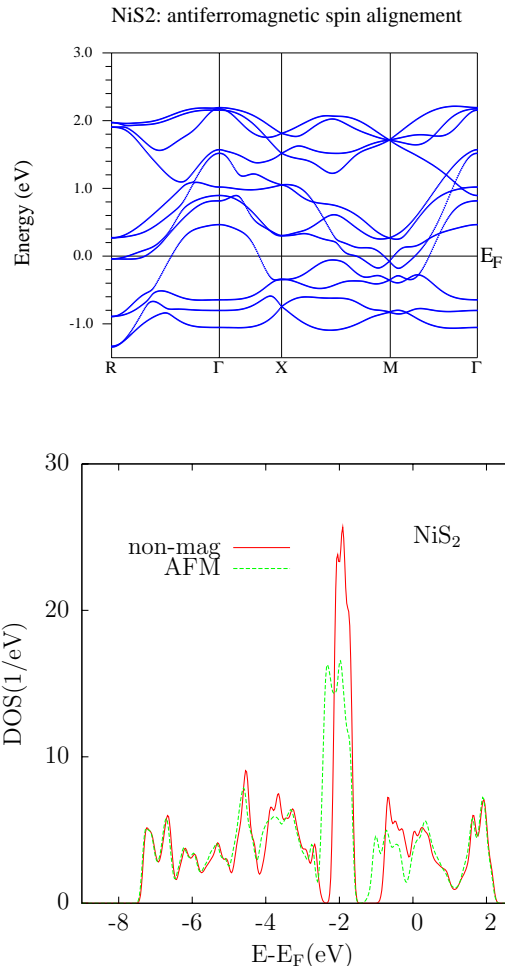


FIG. 4: (Color online) Band structure and density of states of NiS_2 with anti-ferromagnetic spin configuration.

compound	V_{xc}	a (in Å)	mag. order moment (in μ_B)	ΔE in eV	
NiS_2	GGA	5.69	afm	0.73	2.1
NiS_2	LDA	5.69	non	0.20	-0.14
NiS_2	GGA	5.49	non	0.45	0.17
NiS_2	LDA	5.49	non	0.11	-0.17
NiS_2	GGA	5.28	non	0	-
NiSSe	GGA	5.69	afm	0.4	0.034
NiSSe	GGA	5.87	afm	0.5 – 0.6	0.88
NiSSe	LDA	5.87	non	0.1/0.2	-0.14
NiSe_2	GGA	5.96	non	0	-

TABLE II: Magnetic ground state and magnetic moment within LDA/GGA calculations for the systems under investigation. $\Delta E = (E_{\text{non-pol}} - E_{\text{mag}})/(\text{number of Ni})$ is the energy gain due to the magnetic ordering per Ni atom and is given in meV.

IV. GGA+ U , FOCK EXCHANGE

Local approximations to DFT like LDA and GGA fail to describe the insulator [13]. Recently, a variety of insulating transition-metal oxides have been investigated

using LDA+ U [17], LDA+DMFT [14], Fock exchange or hybrid functionals [19], or the GW approximation [26]. In this work, we apply GGA+ U , hybrid functionals, Hartree-Fock, and GW calculations to NiS₂. We use the implementation of GGA+ U , comparing the fully localized limit (SIC) as applied to NiO [17] and the around mean-field treatment (AFM) [27] for the double counting correction, and the EECE treatment [19] within the wien2k code [15].

To start with, we perform constraint GGA calculation to obtain a reasonable value for U . Following the treatment in [28] and assuming a Ni d⁸ configuration as in NiO, we obtain $U_{\text{eff}} = U - J = 6.39$ eV for NiS₂. U_{eff} decreases to 5.89 eV for NiSSe, and further to 4.94 eV for NiSe₂. The different chemistry such leads to a considerable decrease of the correlation energy with doping. With decreasing volume, U_{eff} is constant. In the following, we always use the antiferromagnetic spin structure as discussed in the previous section. The DOS, calculated with $U_{\text{eff}} = 6.4$ eV and the SIC correction, is plotted in Fig. 5, upper panel, and shows a rather poor agreement with experimental data [6, 7]. The Ni 3d states are shifted to too low energies, forming a triple peak structure at the lower band edge. The S 3p states are homogeneously spread over the whole energy range. Using the experimental value of $U = 5$ eV the gap values, namely $\Delta^{\text{SIC}} = 0.6$ eV and $\Delta^{\text{AFM}} = 0.3$ eV, are in the range of the experimental values, but the Ni 3d states are located at -4 eV instead of -2 eV. A similar behavior was found in case of the ferromagnetic metallic pyrite CoS₂ [29].

While GGA+ U is successful for insulators, the description of correlated metals where the requirement of an integer orbital occupation and well established long range order [30] is no longer fulfilled may fail. In case of NiS₂ under pressure, GGA+ U correctly shows that this system is a non-magnetic metal. The results for NiSe₂ on the other hand, are very sensitive to the choice of the method. Using SIC the ground state is a ferromagnetic metal, in case of AFM the antiferromagnetic metal is nearly degenerate to a ferromagnetic metal with two different moments.

In a next step we perform calculation using Fock exchange for the Ni within the muffin tin spheres (exact exchange for correlated electrons, EECE) and LDA for the correlation potential. This approach is known to give quite reasonable results for correlated electron systems [18, 19]. Instead of a parameter U and the choice for the double counting corrections which give deviating results for insulating NiS₂ and metallic NiSe₂, the mixing parameter of the hybrid functional has to be determined. As expected 100 % EECE overestimates the gap by a factor of 5. It also shifts the Ni 3d states to the lower band edge, i. e. to -10 to -8 eV. In this way, 100 % EECE is comparable to $U = 10.7$ eV. The gap is induced within the S p states, and not as expected between the Ni 3d (Mott-Hubbard type) or Ni 3d and S 3p states (charge transfer type). If 25 % EECE is added to LDA the Ni 3d_{2g} states are found at -4 eV. The DOS shape corre-

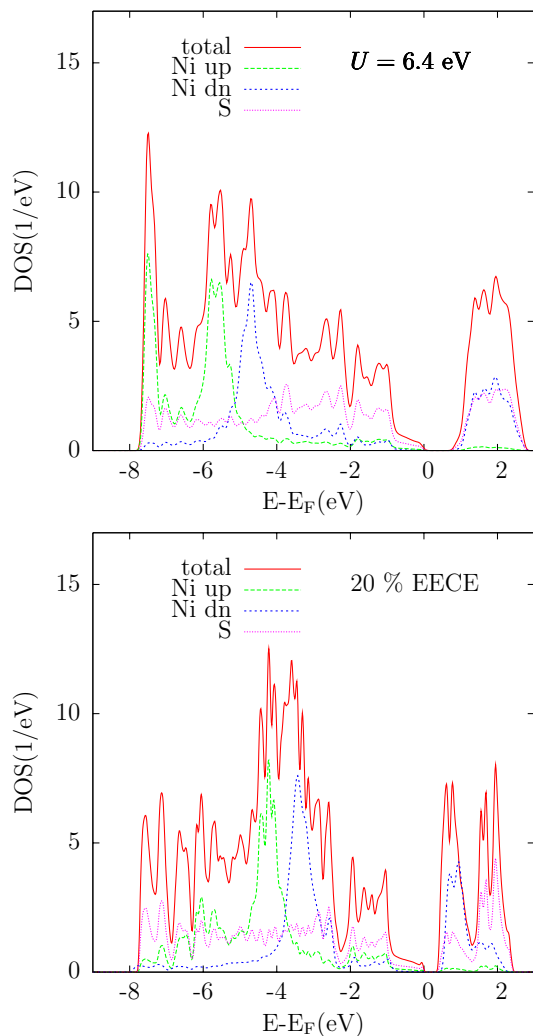


FIG. 5: (Color online) Total density of states of NiS₂ (red line) and contributions of the Ni 3d (green and blue line) and S 3p (pink line) orbitals: we compare the GGA+ U calculation (left-hand side) with the hybrid functional with 20% EECE (right-hand side).

sponds to the DOS obtained for $U = 5.4$ eV (suggested U value from [11]). Decreasing the amount of EECE further, the gap closes below 20%; therefore we perform the following calculation with a hybrid functional where 20% EECE is mixed to LDA. Then, gap in the DOS opens within the Ni-S hybridized states, located between -2 and 1 eV, at the preformed dip in the GGA calculation, as can be seen in Fig. 5. The bonding-antibonding S 3p states dominate at the lower valence and higher conduction band edge. The double peak structure of the empty states observed in XAS can be traced back to a Ni 3d_{eg} double peak and the S 3p antibonding double peak. Using this hybrid functional, an antiferromagnetic solution is obtained, although LDA itself favors the non-magnetic ground state. The calculated moments become smaller under pressure and with doping but do not vanish.

The gap of NiS_2 is very sensitive to the S-S dimer-distance d . Using a structure with $d = 2.15$ Å the band gap amounts to 0.3 eV, whereas it is 0.6 eV with $d = 2.10$ Å. Increasing the dimer distance to $d = 2.36$ Å, i.e. using the structural parameter of NiSe_2 but the lattice constant of NiS_2 , the gap closes. A closer look at the weighted band structure shows that the gap is located at Γ ; the lower band has dominant Ni character, whereas the upper band has dominant S character. The S character of this band shows up only at Γ , compare FeS_2 [12]. According to the band structure the metal-insulator transition under pressure is triggered by the band with Ni character which provides the states at the Fermi level between Γ and X. With doping the metallic state is attributed to the states between X and M. In this way, a metallic ground state is obtained for NiSe_2 due to the increased dimer-distance. On the other hand, reducing the volume also closes the gap at constant dimer-distance. The results for the band structure are shown in Fig. 6, where we compare insulating NiS_2 with metallic NiS_2 under pressure and metallic NiSe_2 .

To summarize, $\text{GGA}+U$ is not able to describe the system properly, neither with the calculated nor estimated U values. Hybrid functionals using Fock exchange can reproduce the insulator and give a reasonable DOS. This approach fails, however, in describing the magnetic phase diagram by overestimating the ordered phase. Thus, we have identified a system where the advantage of hybrid functionals versus $\text{GGA}+U$ can be clearly demonstrated.

V. QUASI-PARTICLE PICTURE: HF AND GW

Corrections to the energy eigenvalues in DFT can be estimated by first order many-body perturbation theory with respect to the difference in exchange correlation self-energy and exchange correlation potential of DFT. Describing the dielectric properties of semiconductors, the GW approximation has become the method of choice [31]. Thereby, the non-local, energy-dependent self-energy is approximated by the Green's function and the screened Coulomb interaction, $\Sigma = \text{GW}$ [32]. The screening is calculated on the level of the random phase approximation. Within the "one-shot" procedure G_0 and W_0 are calculated from LDA/GGA, but this G_0W_0 approach gives appropriate results only if GW is a small correction to LDA. Transition-metal oxides can be treated rather well using self-consistent approaches. For example, the electronic structure of VO_2 is described correctly [26]. Even properties of V_2O_3 can be described [33]. In NiS_2 , the electron-lattice coupling is strong and found to be the driving mechanism of the metal-insulator transition, thus it can be expected that the GW approach is able to provide a description of the insulating state. Similar to VO_2 , in the case of NiS_2 , a self consistent scheme has to be applied to get rid of the metallic starting point. In the following we use the GW implementation of the ABINIT package [21]. We compare, see

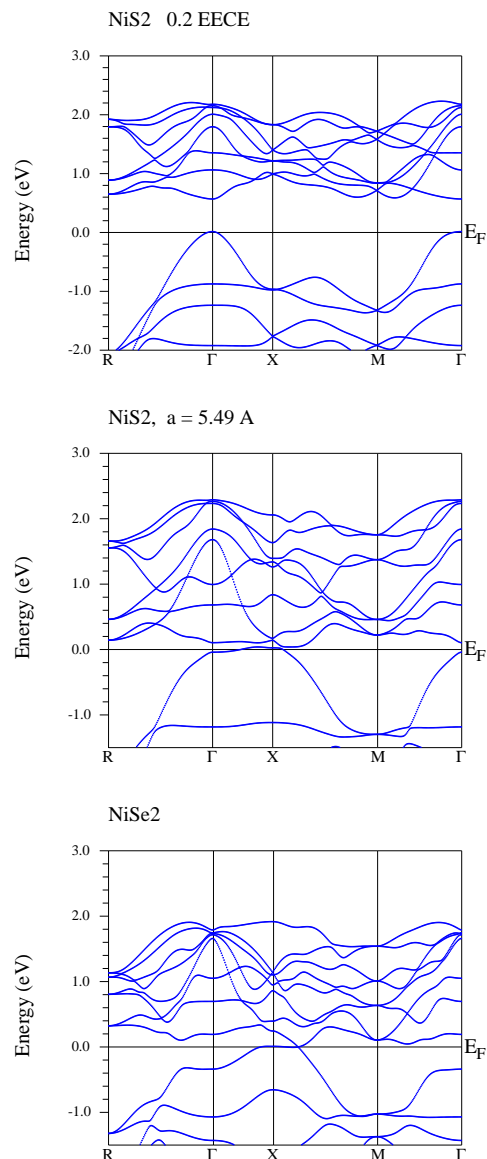


FIG. 6: Band structure obtained using a hybrid functional with 20% EECE. Top: NiS_2 ; middle: NiS_2 under pressure; bottom: NiSe_2 .

[34], Hartree-Fock calculations with self-consistent, but static GW schemes. The self-energy can be written as a sum of the exchange self-energy (static screened exchange), the correlation self-energy (Coulomb-hole term) and the dynamical (energy-dependent) self-energy, and the approximations used within GW are classified along this partitioning. Here, we compare the screened exchange with the screened exchange plus Coulomb-hole. Another static GW approximation is the quasi-particle self-consistent GW [35]. As we start from the Kohn-Sham orbitals obtained within in LDA, spin-polarized calculations are in accordance with non-polarized calculations since LDA favors a non-magnetic ground state. For simplicity we chose the k-points where the correc-

method	spin	k-point	gap
HF	non-pol	Γ	0.3 eV
HF	pol	Γ	0.4 eV
scrEX	pol	M	0.175 eV
COHSEX	non-pol	M	0.021 eV
COHSEX	pol	M	0.025 eV
QPscGW	pol	M	0.027 eV

TABLE III: Energy gaps obtained within different approximation used for the self consistency, namely screened exchange, screened exchange plus Coulomb hole, and model GW [35].

tions are calculated out of the optimal k-set. The given k-points K1 (1/8,1/8,1/8) and K4 (3/8,3/8,3/8) are located between Γ and R, and K2 (3/8,1/8,1/8) and K3 (3/8,3/8,1/8) between X and M. As it can be assumed that the correction do not vary in the vicinity of the chosen k-points, K1 should give the correction at Γ , K2 at X, K3 at M, and K4 at R.

On all GW levels, gaps are induced to the band structure of NiS_2 at the chosen k-points, where the smallest gap occurs at K3 (M). The results are summarized in Tab. III.

The behavior is in accordance with the GGA calculations as we can assign the dip at E_F of the GGA DOS to the bands crossing at M. However, it is found that one band crosses the Fermi level between R and Γ . For this reason, GW calculations cannot describe the insulating state of NiS_2 , even though a gap is formed at all given k-points. Therefore, calculations of compressed NiS_2 and $NiSe_2$ lead to very similar results for the gaps. Moreover, the metallic phases show larger gaps at these k-points, but the crossing is present in each case.

On the other hand, the smallest gap is located at Γ within Hartree-Fock, in accordance with the results discussed in the previous section. In addition, the gap values resulting from the calculations with 20 % EECE and from the Hartree-Fock calculation are astonishingly of similar magnitude. However, the total density of states shows no gap at E_F but a large gap between -5 to -1 eV, despite the direct gaps at the chosen k -points.

As a major shortcoming, the GW and Hartree-Fock calculations, on top of the non-magnetic starting point generated by the LDA, do not generate a magnetic ground state as the EECE does. The local magnetic minimum is thus not obtained.

VI. SUMMARY

In summary, the electronic and magnetic structure of doped and compressed NiS_2 was discussed in great de-

tail within different approximation in the framework of DFT. In particular, LDA/GGA, GGA+ U , and a hybrid functional composed of 20% EECE mixed to LDA have been compared to Hartree-Fock and GW calculations. The metal-insulator transition with applying pressure or doping in NiS_2 can be described properly only when using the hybrid functional. The GGA+ U fails to describe correlated metals since it works only well in case of integer orbital occupation and long range order. However, as the electron-lattice interaction is very strong in NiS_2 , and the results very sensitive to changes in the lattice structure, the results of LDA/GGA calculations already allows to identify the microscopic origin of the metal-insulator transition, namely the dependence on crystal field splitting and bonding-antibonding splitting. Additional corrections to LDA/GGA are then necessary to provide the insulating band structure of NiS_2 .

Therefore, the magnetic properties of NiS_2 , on the other hand, are described best within GGA. LDA underestimates the magnetic order, thus no magnetic ground state is found. The employed hybrid functional overestimates the magnetic order, even when only a small amount of Fock exchange is mixed to LDA. The GGA+ U approach cannot capture the magnetic properties as expected for metallic compounds away from half band filling.

Thus, the Fock exchange applied to the transition metal Ni in the EECE approach gives reasonable results as compared to experimental data as far as the electronic properties are concerned as well as in the insulating as the metallic phases of NiS_2 . The ordering of the magnetic moments is highly overestimated. The magnetic order present in the EECE approach alters the band structure in comparison to Hartree-Fock.

Acknowledgments

We acknowledge fruitful discussions with L. Baldassarre, U. Eckern, V. Eyert, M. Gatti, and J. Kuneš. Some of the presented results have been obtained through the use of the ABINIT code, a common project of the Université Catholique de Louvain, Corning Incorporated, and other contributors (URL <http://www.abinit.org>). The pseudo-potentials were provided by S. Botti and M. Gatti. Financial support was provided by the Deutsche Forschungsgemeinschaft (SFB 484)

[1] F. Gautier, G. Krill, M. F. Lapierre, P. Panissod, C. Robert, G. Czjzek, J. Fink, and H. Schmidt, Phys. Lett. **53A**, 31 (1975).

[2] J. A. Wilson and G. D. Pitt, Phil. Mag. **23**, 1297 (1971).

[3] Y. Sekine, H. Takahashi, N. Mōri, T. Matsumoto, and T. Kosaka, Physica B: Condensed Matter **237-238**, 148

- (1997)
- [4] R. L. Kautz, M. S. Dresselhaus, D. Adler, and A. Linz, *Phys. Rev. B* **6**, 2078 (1972).
- [5] A. Y. Matsuura, Z.-X. Shen, D. S. Dessau, C.-H. Park, T. Thio, J. W. Bennett, and O. Jepsen, *Phys. Rev. B* **53**, R7584 (1996).
- [6] L. Sangaletti, F. Parmigiani, T. Thio, and J. W. Bennett, *Phys. Rev. B* **55**, 9514 (1997).
- [7] K. Mamiya *et. al.*, *Phys. Rev. B* **58**, 9611 (1998).
- [8] S. R. Krishnakumar and D. D. Sarma, *Phys. Rev. B* **68**, 155110 (2003).
- [9] D. D. Sarma, S. R. Krishnakumar, E. Weschke, C. Schüßler-Langeheine, C. Mazumdar, L. Kilian, G. Kaindl, K. Mamiya, S.-I. Fujimori, A. Fujimori, and T. Miyadai, *Phys. Rev. B* **67**, 155112 (2003).
- [10] J. M. Tomczak and S. Biermann, *J. Phys.: Condens. Matter* **21**, 064209 (2009).
- [11] W. Folkerts, G. A. Sawatzky, C. Haas, R. A. de Groot, and H. U. Hillebrecht, *J. Phys. C* **20**, 4135 (1987).
- [12] V. Eyert, K.-H. Höck, S. Fiechter, and H. Tributsch, *Phys. Rev. B* **57**, 6350 (1998).
- [13] A. Perucchi, C. Marini, M. Valentini, P. Postorino, R. Soprocase, P. Dore, P. Hansmann, O. Jepsen, G. Sangiovanni, A. Toschi, K. Held, D. Topwal, D. D. Sarma, and S. Lupi, *Phys. Rev. B* **80**, 073101 (2009).
- [14] J. Kuneš, L. Baldassarre, B. Schachner, C. A. Kuntscher, Dm. M. Korotin, V. I. Anisimov, arXiv:0907.2154
- [15] P. Blaha, K. Schwarz, G. Madsen, D. Kvasicka, and J. Luitz, *Wien2k: An augmented plane wave + local orbitals program for calculating crystal properties*, Vienna University of Technology, 2001.
- [16] J. P. Perdew, K. Burke, and M. Ernzerhof, *Phys. Rev. Lett.* **77**, 3865 (1996).
- [17] V. I. Anisimov, I. V. Solovyev, M. A. Korotin, M. T. Czyzyk, and G. A. Sawatzky, *Phys. Rev. B* **48**, 16929 (1993); V. I. Anisimov, D. Bukhvalov, and T. M. Rice, *Phys. Rev. B* **59**, 7901 (1999).
- [18] P. Novák, J. Kuneš, L. Chaput, and W. E. Pickett, *phys. stat. sol. (b)* **243**, 563 (2006).
- [19] F. Tran, P. Blaha, K. Schwarz, *Phys. Rev. B* **74**, 155108 (2006).
- [20] X. Gonze, J.-M. Beuken, R. Caracas, F. Detraux, M. Fuchs, G.-M. Rignanese, L. Sindic, M. Verstraete, G. Zerah, F. Jollet, M. Torrent, A. Roy, M. Mikami, Ph. Ghosez, J.-Y. Raty, and D. C. Allan, *Comp. Mat. Sci.* **25**, 478 (2002).
- [21] X. Gonze, G.-M. Rignanese, M. Verstraete, J.-M. Beuken, Y. Pouillon, R. Caracas, F. Jollet, M. Torrent, G. Zerah, M. Mikami, Ph. Ghosez, M. Veithen, J.-Y. Raty, V. Olevano, F. Bruneval, L. Reining, R. Godby, G. Onida, D. R. Hamann, and D. C. Allan, *Zeit. Kristallogr.* **220**, 558 (2005).
- [22] T. A. Bither, R. J. Bouchard, W. H. Cloud, P. C. Donohue, and W. J. Siemons, *Inorg. Chem.* **7**, 2208 (1968).
- [23] K. Iwaya, Y. Kohsaka, S. Satow, T. Hanaguri, S. Miyasaka, and H. Takagi, *Phys. Rev. B* **70**, 161103 (2004).
- [24] P. Kwizera, M. S. Dresselhaus, and D. Adler, *Phys. Rev. B* **21**, 2328 (1980).
- [25] R. Hafner, D. Spisk, R. Lorenz, and J. Hafner, *J. Phys.: Condens. Matter* **13** L239 (2001).
- [26] M. Gatti, F. Bruneval, V. Olevano, and L. Reining, *Phys. Rev. Lett.* **99**, 266402 (2007).
- [27] M. T. Czyzyk and G. A. Sawatzky, *Phys. Rev. B* **49**, 14211 (1994).
- [28] G. K. H. Madsen and P. Novák, *EPL* **69**, 777 (2005).
- [29] S. K. Kwon, S. J. Youn, and B. I. Min, *Phys. Rev. B* **62**, 357 (2000).
- [30] I. S. Elfimov, G. A. Sawatzky, A. Damascelli, *Phys. Rev. B* **77**, 060504 (R)
- [31] W. G. Aulbur, L. Jönsson, and J. Wilkins, in *Solid State Physics*, edited by H. Ehrenreich and F. Seipen (Academic Press, New York, 2000), Vol. 54, p. 1.
- [32] L. Hedin, *Phys. Rev.* **139**, A796 (1965).
- [33] E. Papalazarou, M. Gatti, M. Marsi, V. Brouet, F. Iori, L. Reining, E. Annese, I. Vobornik, F. Offi, A. Fondacaro, S. Huotari, P. Lacovig, O. Tjernberg, N. B. Brookes, M. Sacchi, P. Metcalf, and G. Panaccione, arXiv:0903.4303
- [34] F. Bruneval, N. Vast, and L. Reining, *Phys. Rev. B* **74**, 045102 (2006).
- [35] S. V. Faleev, M. van Schilfgaarde, and T. Kotani, *Phys. Rev. Lett.* **93**, 126406 (2004).

NiSe2 0.2 EECE

